

Strongly emissive plasma-facing material under space-charge limited regime: Application to emissive probes

Jordan Cavalier, Nicolas Lemoine, Guillaume Bousselein, Nicolas Plihon, and Jordan Ledig

Citation: *Physics of Plasmas* **24**, 013506 (2017); doi: 10.1063/1.4973557

View online: <http://dx.doi.org/10.1063/1.4973557>

View Table of Contents: <http://aip.scitation.org/toc/php/24/1>

Published by the *American Institute of Physics*

Articles you may be interested in

[Kinetic modeling of Langmuir probe characteristics in a laboratory plasma near a conducting body](#)
Physics of Plasmas **24**, 012901 (2017); 10.1063/1.4972879

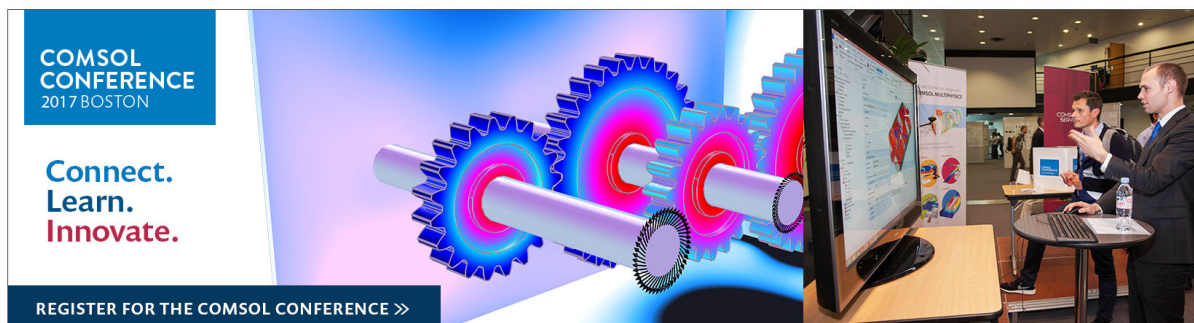
[Characteristics of floating potential of a probe in electronegative plasma](#)
Physics of Plasmas **24**, 013507 (2017); 10.1063/1.4973653

[Pulsed floating-type Langmuir probe for measurements of electron energy distribution function in plasmas](#)
Physics of Plasmas **24**, 013508 (2017); 10.1063/1.4972576

[Floating potential measurements in plasmas: From dust to spacecraft](#)
Physics of Plasmas **24**, 023701 (2017); 10.1063/1.4975610

[Experimental and theoretical study of an atmospheric air plasma-jet](#)
Physics of Plasmas **24**, 013502 (2017); 10.1063/1.4973555

[Orbital motion theory and operational regimes for cylindrical emissive probes](#)
Physics of Plasmas **24**, 023504 (2017); 10.1063/1.4975088



Strongly emissive plasma-facing material under space-charge limited regime: Application to emissive probes

Jordan Cavalier,^{1,2} Nicolas Lemoine,² Guillaume Bousselein,³ Nicolas Plihon,³
 and Jordan Ledig²

¹*Institute of Plasma Physics, AS CR, v.v.i, Za Slovankou 3, Prague 8, Czech Republic*

²*Institut Jean Lamour IJL, Université de Lorraine, UMR 7198 CNRS, Vandœuvre-lès-Nancy, France*

³*Univ Lyon, Ens de Lyon, Univ Claude Bernard, CNRS, Laboratoire de Physique, F-69342 Lyon, France*

(Received 20 September 2016; accepted 19 December 2016; published online 6 January 2017)

A quasi-static theoretical 1D model is developed to describe the sheath structure of a strongly emissive plasma-facing material and is subsequently applied to emissive probes' experimental data—which are usually supposed to be an efficient tool to directly measure plasma potential fluctuations. The model is derived following the space-charge limited emission current model developed in Takamura *et al.*, [Contrib. Plasma Phys. **44**(1–3), 126–137 (2004)], adding the contribution of secondary emission due to back-diffusion of plasma electrons at the emitting surface. From this theory, current-voltage characteristics of emissive probes are derived. A theoretical relation between the floating potential of an emissive probe and plasma parameters is obtained and a criterion is derived to determine the threshold between the thermoemission limited current regime and space-charge limited current regime. In the space-charge limited regime, a first order expansion is then applied to the quasi-static relation to study the effect of plasma fluctuations on emissive probe measurements. Both the mean values and the fluctuations of the floating potential of an emissive probe predicted by the model, as well as the potential value at which the transition between emission current regimes occurs, are compared to three sets of experimental data obtained in two different plasma devices. *Published by AIP Publishing.* [<http://dx.doi.org/10.1063/1.4973557>]

I. INTRODUCTION

The study of electron emitting surfaces is of great interest for plasma physics. First, an emissive enough floating conducting surface has a mean electric potential close to that of the surrounding plasma. This has led to the wide use of emissive probes^{20,21} in which the floating potential of a strongly emissive material is interpreted as a direct measurement of plasma potential—up to frequencies low compared to the ion plasma frequency. Second, when a surface becomes emissive, emitted electrons modify the electric potential in the sheath ahead, which in turn affect thermal fluxes on the surface. This question has strong implications in the field of magnetic controlled fusion. For instance, the divertor in ITER (that will receive most of the thermal flux from the plasma) is expected to reach temperatures so high that it could be strongly emissive.

A precise understanding of the sheath structure facing emissive material surface is thus required to model incident particles and heat fluxes on the surface. Restricting ourselves to electrostatic probes, this is a recurrent problem for the analysis of emissive probes heated by an external controlled process, often used in low-temperature plasmas to measure the plasma potential and its low-frequency fluctuations.²⁰ This is also an important issue for reciprocating probes, used to study edge plasma in tokamaks, which are plunged during a very short time into hot plasmas that makes them occasionally self-emissive.² In the context of fusion plasmas, a precise estimation of particle and heat transport requires a precise measurement of the phase between plasma density and plasma potential fluctuations, and emissive probes are

considered for the measurement of the latest (see the undergoing development of a probe head for TCV and ASDEX UG plasma devices under the WPMST2 project¹ and a newly developed emissive probe¹⁸). A precise understanding of the behavior of emissive probe is thus a key issue when addressing turbulent plasma transport, especially in the case of drift wave turbulence.

While it is now widely accepted that the time-averaged value of the floating potential of emissive probes can equal the surrounding plasma potential in cold plasmas,³ it has been recently shown that the fluctuations of the floating potential can differ significantly from the fluctuations of the plasma potential, both in phase and amplitude.^{4,5} Moreover, the experimental investigation reported in Ref. 5 demonstrated that the fluctuation level of the floating potential of emissive probes follows a thermoemission limited current model only for low emission currents. Above a critical value of the emission current, fluctuations of the floating potential go clearly off the model curve. This non-monotonic evolution of the floating potential evolution is suspected to be the signature of a transition to a space-charge limited current regime.

In this article, we develop a theoretical framework to account for the above two observations. More specifically, we derive current-voltage characteristics of emissive probes in the space-charge limited regime, as the classical model for thermoemission limited current regime did not account for experimental measurements described in Refs. 4 and 5. The thermoemission regime exists as long as the potential profile in the sheath is monotonic (see Fig. 1(a)), so that the

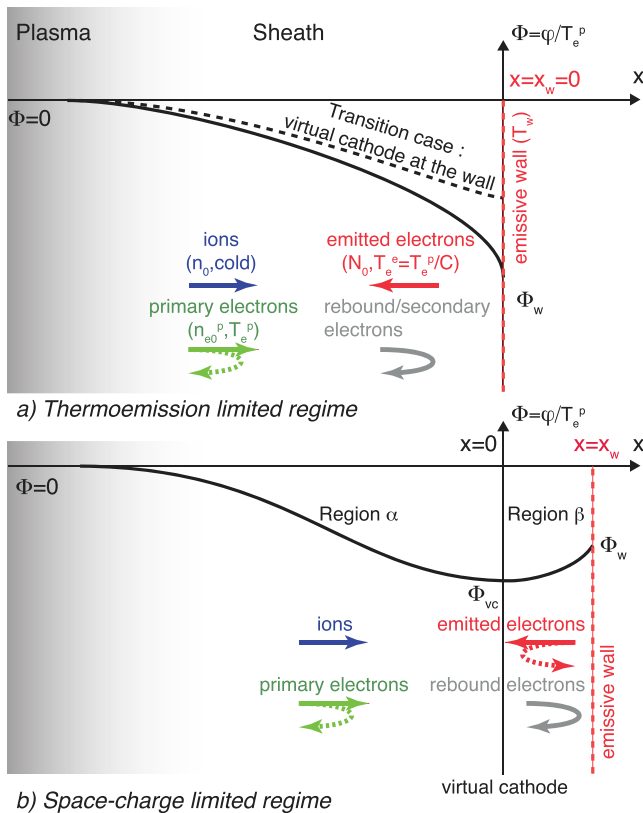


FIG. 1. Schematic of 1-D static sheath under (a) thermoemission limited regime (b) space-charge limited regime. See text for details.

emission current density reaching the plasma is only limited by the wall emissivity (usually controlled by its temperature). The transition to the space-charge regime is observed when the low energy electrons emitted from the surface would have a too high current density or would not be accelerated enough by the sheath drop, so that their density at the plasma/sheath edge would be too large and, eventually, break plasma quasineutrality, if the potential profile were to be monotonic. Before that occurs, a virtual cathode appears in front of the wall that has a lower potential than the wall potential. It filters out the low energy emitted electrons in such a way that a given current density of passing emitted electrons is associated with a lower density at the plasma/sheath boundary. Note that the potential drop also repels a fraction of incoming electrons. The existence of virtual cathodes was postulated and demonstrated by the pioneering work of Langmuir,¹² and then investigated in details by Kemp and Sellen.¹⁰ More recently, detailed measurements of virtual cathode structures caused by secondary electron emission¹³ have been reported in low density plasmas. In this article, we extend the work presented in Ref. 23 by adding the effect of secondary electron emission by retrodiffusion of primary electrons. The addition of this new ingredient is motivated by the fact that between 10% and 40% of primary electrons reaching a tungsten wall could bounce on it.¹¹ Recently, even larger values have been measured on the carbon fiber composite (CFC) component in the plasma edge of a tokamak.⁸ This has implication on the mean floating potential value of the probe as well as on its

fluctuations as the rebound current would follow plasma fluctuations. The model developed in this work enables us to provide predictions for the relations between fluctuations of the floating potential of emissive probes and fluctuations of the plasma potential in the space-charge regime. It is then compared to experimental results.

The article is organized as follows. In Section II, a model for the space-charge limited emission current regime is derived, following the calculation given in Ref. 23 and adding retrodiffusion of primary electrons. In this section, we also derive an analytical expression of the potential drop between the wall and the virtual cathode potentials. We then show how to obtain I - V characteristics from the model and discuss the implications of the rebound electrons on the sheath characteristics, and hence floating potentials, virtual cathode potential drop or particles fluxes at the emissive surface. In Sections III and IV, this model is compared to experimental results. In Section III, the onset temperature at which the emissive wall enters the space-charge limited regime is derived and compared to experimental data from emissive probes. In Section IV, we compare fluctuations from the space-charge model developed in this article and experimental data. In Section V, results are discussed and we come to a conclusion.

II. CURRENT LIMITED BY SPACE-CHARGE REGIME

This section is devoted to the derivation of a 1D model of a plasma sheath in front of an emissive wall when the emission current is large enough to be limited by the space-charge effect. In short, when the current density of electron emitted from the wall is low enough, the potential profile in the sheath is monotonic; this regime is usually referred to as the *thermoemission current limited regime* since the amount of emitted electrons reaching the plasma is controlled by the emissivity of the wall (which is usually set by the temperature for a given type of emissive material such as tungsten or LaB₆). On the other hand, when the current density of electron emitted from the wall is large enough, the potential profile in the sheath is non monotonic. The minimum value of the potential profile is no more reached at the wall, but within the sheath, giving rise to a so-called *virtual cathode* (in other words, this is obtained when the equilibrium relations require a negative electric field at the wall). The existence of this virtual cathode leads to a reflection of part of the emitted electrons back to the wall; this regime is usually referred to as the *space-charge current limited regime* since the amount of emitted electrons reaching the plasma is mainly controlled by the potential drop between the wall potential and the virtual cathode. Fig. 1 shows a schematic view of the sheath structure and associated particles fluxes in both regimes, in which the minimum of the sheath potential is located at $x = 0$. Fig. 1(a) displays the thermoemission current limited regime: the potential profile is monotonic and the electric is oriented towards the wall at the wall location. Fig. 1(b) displays the space-charge current limited regime: the potential profile is non-monotonic and the electric is oriented outwards of the wall at the wall location. The transition between both regimes is observed for a zero electric field at

the wall. In the remaining of this section, one will restrict oneself to the space-charge current limited regime and derive a model for the sheath including rebound electrons, which are shown to strongly influence the sheath characteristics.

A. Hypothesis of the model and outline

Most of the hypothesis and conventions necessary for the derivation of this model are summarized in Fig. 1(b), which displays typical spatial evolutions of the sheath potential. A hot emissive wall at a wall temperature T_w and potential φ_w is facing a plasma, supposed to be at infinity, of density n_0 , whose plasma potential is φ_p . The distribution function of electrons from the plasma is assumed to be a Maxwellian with electron plasma temperature T_e^p and the ions, of mass m_i , are considered cold. A Maxwellian distribution function is also assumed for the electrons emitted by the hot emissive wall, with a temperature $T_e^e = T_e^p/C$. We assume that the plasma is hot enough so that T_e^p is greater than T_e^e , and hence the constant C is greater than one. Note also that T_e^e could differ from T_w . In the remaining, the superscript p stands for *plasma* or *primary* electrons, and the superscript e stands for *emitted* electrons at the wall, while Takamura and co-workers used a superscript s standing for *secondary* electrons; our choice was motivated to avoid confusion with true secondary emission. The sheath is assumed to be collisionless, implying energy and flux conservation. The electron mass will be denoted as m_e , and the elementary charge as e . Normalized potentials Φ are defined as $\Phi = (\varphi - \varphi_p)/T_e^p$; dimensional potentials and temperatures are given in volts and in electron-volts, respectively.

For simplicity, the problem is assumed to be one dimensional and static. The hot emitting surface emits a sufficient amount of electrons so that a drop of potential occurs in front of the wall. The space potential $\Phi(x)$ is equal to Φ_w at the wall location $x = x_w \geq 0$ and reaches a minimum Φ_{vc} at the virtual cathode location $x = 0$. The sheath entrance or plasma limit is at $x \rightarrow -\infty$. Following the notations of Ref. 23 (see also Fig. 1(b)), the sheath region at $x < 0$ is labeled α (i.e., between the plasma and the virtual cathode), while the sheath region at $x > 0$ is labeled β (i.e., between the virtual cathode and the wall).

We follow the lead of Takamura and co-workers²³ and add to the calculation a new population of electrons: the primary electrons that have rebounded elastically on the material as their contribution could be non-negligible. As a novelty, we also derive a model for the potential of a floating material by establishing numerically the dependence of the virtual cathode potential with the different plasma parameters. In addition, we give a method for calculating the emission electron temperature at which the transition occurs between current limited by thermoelectron emission and the space-charge limited regime.

For the sake of clarity, and before detailing the derivation, we first provide a brief outline in Subsections II B–II E which establish a relation between Φ_w and Φ_{vc} , as well as a framework for numerical integration of I – V characteristic of emissive probes in the space-charged limited regime. From the dynamics of charged particle populations in regions α and

β , we seek expressions of the current densities associated with each of these populations in Subsection II B. In Subsection II C, these current densities are then expressed as a function of Φ_{vc} , Φ_w , M , γ , where M is the Mach number and γ is the ratio of passing emitted electrons current density over the passing plasma electron current density. In Subsection II D, a modified Bohm criterion, derived from Poisson's equation in region α , enables us to express M as a function of γ and Φ_{vc} , and a relation between γ and Φ_{vc} is also obtained from the condition of zero electric field at the virtual cathode (or equivalently minimum of potential). Finally, in Subsection II E, matching the current densities computed for each population at the virtual cathode leads to an explicit relation between Φ_{vc} and Φ_w that leads to a theoretical expression of the wall floating potential or to numerical integration of I – V characteristic of emissive probes under the space-charge regime.

B. Densities in region α and current densities of passing particles

In this subsection, particle densities for each population are expressed in the region α . The current densities of passing particles, those able to override the potential barrier created by the virtual cathode, are then derived.

1. Cold plasma ions

Let us first deal with the dynamics of ions. Assuming that cold ions of mass m_i are accelerated from the plasma in the sheath potential with no collisions, the ion density $n_i(x)$ and ion velocity $v_i(x)$ are derived from flux conservation $d(n_i v_i)/dx = 0$ and energy conservation $m_i v_i(x)^2 + 2eT_e^p \Phi(x) = Cte$, as

$$\begin{aligned} v_i(x) &= \sqrt{V_0^2 - \frac{2eT_e^p \Phi(x)}{m_i}} \quad \text{and} \\ n_i(x) &= n_0 \left(1 - \frac{2\Phi(x)}{M^2}\right)^{-1/2}, \end{aligned} \quad (1)$$

where n_0 is the ion density in the plasma (at $x \rightarrow -\infty$), V_0 is the ion velocity at the sheath entrance, and the Mach number at the sheath entrance M is defined as $M = V_0/c_s$ with the sound speed $c_s = \sqrt{eT_e^p/m_i k_B}$, k_B being the Boltzmann constant. Since ions are collisionless, the ion current density $j_i(x)$ is constant in the region α and reads

$$j_i(x) = j_{is} = en_0 M c_s, \quad (2)$$

where j_{is} is the ion saturation current.

2. Electrons emitted by the wall

In the space-charge limited regime, only part of the electrons emitted by the wall, those having a sufficiently high velocity to override the virtual cathode potential barrier ($\Phi_{vc} - \Phi_w$), reach the α region. The calculation, detailed in the work by Takamura and coworkers,²³ is only briefly recalled here. Assuming energy and flux conservation and a Maxwellian distribution function $f^e(v_e)$ of emitted electrons at the wall location $x = x_w$, the density of passing emitted electrons reads

$$n_{e,\text{pass}}^e(x) = \frac{N_0}{2} \operatorname{erfc}\left(\sqrt{C(\Phi(x) - \Phi_{vc})}\right) \exp(C(\Phi(x) - \Phi_w)), \quad (3)$$

where N_0 is the emitted electron density at the wall and $\operatorname{erfc}(y)$ the complementary error function defined as $\sqrt{\pi}/(4b) \operatorname{erfc}(a\sqrt{b}) = \int_a^{+\infty} e^{-bx^2} dx$. It is worth emphasizing that the above expression for the density of emitted electrons $n_{e,\text{pass}}^e$ is the total density of emitted electrons in region α , while it only represents part of the emitted electrons density in region β . The mean velocity of passing electrons is then computed as

$$\begin{aligned} \langle v_e^e \rangle_{\text{pass}} &= - \frac{\int_{-\infty}^{-v_{\min}^e} v_e f^e(v_e) dv_e}{\int_{-\infty}^{-v_{\min}^e} f^e(v_e) dv_e} \\ &= - \sqrt{\frac{2T_e^e}{\pi m_e}} \frac{\exp(-C(\Phi(x) - \Phi_{vc}))}{\operatorname{erfc}\left(\sqrt{C(\Phi(x) - \Phi_{vc})}\right)}, \end{aligned} \quad (4)$$

where $v_{\min}^e = \sqrt{eT_e^p(\Phi_w - \Phi_{vc})/m_e}$ is the minimum velocity necessary for an electron emitted at the surface to override the virtual cathode potential barrier. The current density of passing emitted electrons reads

$$j_{e,\text{pass}}^e = en_{e,\text{pass}}^e \langle v_e^e \rangle_{\text{pass}} = \frac{1}{2} eN_0 \sqrt{\frac{2eT_e^e}{\pi k_B m_e}} \exp(C(\Phi_{vc} - \Phi_w)). \quad (5)$$

It is this emission current that contributes to the probe current as the non-passing electrons are counted once positively when leaving the wall and once negatively when returning, resulting in a zero net current. This current is also called the space-charged limited current.

3. Primary plasma electrons

In the region α between the plasma and the virtual cathode, the primary electrons are in equilibrium under the action of an electrostatic field and therefore their density follows the Boltzmann law $n_e^p(x) = n_{e0}^p \exp(\Phi(x))$, where n_{e0}^p is the primary electron density at $x \rightarrow -\infty$. Note that $n_{e0}^p \neq n_0$ as some electrons coming from the emissive wall (either emitted or rebound electrons) are also present in the plasma and are to be accounted for quasi-neutrality. The density $n_{e,\text{pass}}^p$ and the density current $j_{e,\text{pass}}^p$ of passing primary electrons are also estimated similarly to the derivation of Eq. (3), as

$$\begin{aligned} n_{e,\text{pass}}^p(x) &= \frac{n_{e0}^p}{2} \operatorname{erfc}\left(\sqrt{\Phi(x) - \Phi_{vc}}\right) \exp(\Phi(x)) \quad \text{and} \\ j_{e,\text{pass}}^p &= \frac{1}{2} en_{e0}^p \sqrt{\frac{2eT_e^p}{\pi k_B m_e}} \exp(\Phi_{vc}). \end{aligned} \quad (6)$$

4. Rebound electrons

We now add a new ingredient that was not incorporated in the work by Takamura and coworkers²³ by considering the part of primary electrons that elastically collides with the

wall and go backward. The contribution of such electrons to the total current can be non-negligible as between 10% and 40% of primary electrons reaching a tungsten wall bounce on it,¹¹ and up to 80% at low plasma temperature according to Ref. 8 for CFC wall in tokamaks. Moreover, as we consider collisions to be elastic, all primary electrons bouncing on the wall have a sufficiently high kinetic energy to override the potential barrier again. Thus, the rebound electron density at the wall location x_w is defined as $n_e^r(x_w) = -\gamma_r n_{e,\text{pass}}^p(x_w)$ with γ_r the rebound coefficient believed to be between 0.1 and 0.4 as previously stated. Assuming elastic collisions and flux conservation, the current density of rebound electrons is defined as $j_e^r = -\gamma_r j_{e,\text{pass}}^p$, and this equality holds everywhere, leading to

$$j_e^r = -\frac{\gamma_r}{2} en_{e0}^p \sqrt{\frac{2eT_e^p}{\pi k_B m_e}} \exp(\Phi_{vc}). \quad (7)$$

5. True secondary emission

In this model, the contribution of true secondary electrons is not taken into account. The reason is the following. Secondary electrons are created by collisions with the wall either of passing primary electrons either of returning emitted electrons not able to override the potential barrier. Secondary electrons that are created from passing primary electrons $j_{e,\text{pass}}^p$ lead to a very small current at the wall compared to the emitted current (which will be verified *a posteriori* in Section II E), and thus those passing secondary electrons are a small fraction of the total passing electrons. Very few secondary electrons are created by low energy emitted electrons that bounce in the virtual cathode and come back to the wall as their temperature is low ($T_e^e \sim 0.3$ eV maximum) leading to a secondary emission coefficient close to zero.¹¹ Thus, true secondary emission is to be taken into account only in regimes where emission current is temperature limited.

C. Determination of edge densities

Before using the different densities in Poisson's equation, one can notice that two constants are to be determined: the density of emitted electrons at the surface N_0 and the density of primary electrons at the plasma/sheath boundary n_{e0} . Quasineutrality at the plasma/sheath edge leads to the relation

$$n_0 = n_{e0}^p + n_{e,\text{pass}}^e(-\infty) + n_e^r(-\infty), \quad (8)$$

where we recall that n_0 is the plasma ion density. It is useful to define the ratio γ as the ratio of the passing emitted electron current density over the passing plasma electron current density as $\gamma = -j_{e,\text{pass}}^e/j_{e,\text{pass}}^p$. This γ coefficient is similar to the true secondary γ_s or rebound γ_r emission and may be understood as an effective coefficient linking the emitted electron current density reaching the plasma with the plasma electron current density reaching the wall in the presence of a virtual cathode. Quasineutrality leads to the following relations:

$$\begin{cases} N_0 = \gamma n_{e0}^p C^{-1/2} \exp(\Phi_{vc} + (\Phi_w - \Phi_{vc})/C) \\ n_{e0}^p = \frac{n_0}{1 + AG + A_r G \gamma_r / \gamma}, \end{cases} \quad (9)$$

with

$$\begin{cases} A = \sqrt{-\pi C \Phi_{vc}} \operatorname{erfc}(\sqrt{-C \Phi_{vc}}) \exp(-C \Phi_{vc}) \\ G = \frac{\gamma}{2} (-\pi \Phi_{vc})^{-1/2} \exp(\Phi_{vc}) \\ A_r = \sqrt{-\pi \Phi_{vc}} \operatorname{erfc}(\sqrt{-\Phi_{vc}}) \exp(-\Phi_{vc}). \end{cases} \quad (10)$$

D. Bohm criterion

The previous analysis shows that there are still four independent parameters for estimating the different currents: the Mach number M , the ratio γ , the virtual cathode potential Φ_{vc} , and the wall potential Φ_w such that the total density current flowing through the wall can be expressed as $j_{tot} = f(M, \gamma, \Phi_{vc}, \Phi_w)$. In this section, a modified Bohm criterion, classically established by integration of the Poisson's equation, settles M as a function of Φ_{vc} and G —or equivalently as a function of Φ_{vc} and γ from Eq. (10). Moreover, using the fact that the virtual cathode is a local minimum of the potential (equivalently that the electric field is zero at the virtual cathode) leads to express γ as a function of Φ_{vc} . Finally, the total current density may be expressed as a function of Φ_w and Φ_{vc} , allowing for the computation of the floating potential of the hot wall or for the computation of the I - V characteristic of emissive probes.

Introducing ξ as the space variable normalized to the Debye length $\lambda_D = \sqrt{\epsilon_0 e T_e^p / (n_0 k_B)}$ with ϵ_0 the vacuum permittivity, Poisson's equation in region α reads

$$\begin{aligned} \frac{d^2 \Phi(\xi)}{d\xi^2} = & -\frac{1}{\sqrt{1 - \frac{2\Phi(\xi)}{M^2}}} + \frac{1}{1 + AG + A_r G \gamma_r / \gamma} \\ & \times \left[e^{\Phi(\xi)} \left(1 + \frac{\gamma_r}{2} \operatorname{erfc}(\sqrt{\Phi(\xi) - \Phi_{vc}}) \right) \right. \\ & \left. + G \sqrt{-\pi \Phi_{vc}} C e^{C(\Phi(\xi) - \Phi_{vc})} \operatorname{erfc}(\sqrt{C(\Phi(\xi) - \Phi_{vc})}) \right]. \end{aligned} \quad (11)$$

This equation can be integrated between $-\infty$ and ξ by multiplying each side by $d\Phi/d\xi$ and employing zero electric field at the plasma/sheath edge as boundary conditions. As the left hand side $(d\Phi/d\xi)^2$ is always positive, a solution of this equation only exists if the right hand side is positive as well. This implies a condition on the Mach number M and so on the ion velocity at the entrance of the sheath. Such a condition can be found by making a second order Taylor expansion of the right hand side near the sheath edge $x \rightarrow -\infty$, where Φ and $d\Phi/d\xi$ tend to zero. We then find a modified Bohm condition for a stable sheath formation which is

$$M^2 \geq \frac{1 + AG + A_r G \gamma_r / \gamma}{1 + C(A - 1)G + G^2(A_r - 1)\gamma_r^2 / \gamma^2}. \quad (12)$$

This criterion is similar to the one obtained in Ref. 23, with additional terms accounting for rebound electrons. Using the fact that the electric field is zero at the virtual cathode (i.e., $d\Phi/d\xi(\Phi = \Phi_{vc}) = 0$) and using the marginal condition for the Bohm criterion (i.e., equality condition in Eq. (12)) a fourth order polynomial expression in γ (through G) is obtained as

$$\begin{aligned} & (1 + C(A - 1)G + G^2(A_r - 1)\gamma_r^2 / \gamma^2) \\ & \times (\beta_0 + \beta_1 G + \beta_2 G^2 + \beta_3 G^3) = 0, \end{aligned} \quad (13)$$

where $\beta_0, \beta_1, \beta_2$, and β_3 are coefficients that are not specified for conciseness and that depend on A and C and thus only on Φ_{vc} and on the plasma parameters. Solving this polynomial expression allows us to express γ as a function of Φ_{vc} , so that both γ and M are only functions of Φ_{vc} . Roots of $1 + C(A - 1)G + G^2(A_r - 1)\gamma_r^2 / \gamma^2$ have no physical meaning because it corresponds to $M \rightarrow +\infty$ (Eq. (12)). The right-hand part of Eq. (13) can be solved by the Cardan method. It has a positive discriminant and thus three real solutions, from which only one satisfies $G > 0$ (see Eq. (10)).

E. Relation between Φ_w and Φ_{vc}

Plugging N_0 from Eq. (9) in Eq. (5) allows us to rewrite the current density of passing emitted electrons as

$$j_{e,pass}^e = j_{is} \left[\frac{G}{1 + AG + A_r G \gamma_r / \gamma} \sqrt{-2 \frac{m_i}{m_e} \Phi_{vc}} \right]. \quad (14)$$

This current density may also be expressed using the Richardson-Dushman's formula. The emitted current density at the wall $x = x_w$ is given by

$$j_{e,wall} = \frac{A_0}{2} T_w^2 \exp\left(-\frac{\varphi_{work}}{T_w}\right), \quad (15)$$

where A_0 the Dushman's constant and φ_{work} the so-called work function.

Accounting for the drop of potential in front of the wall, the current density of passing emitted electrons at the virtual cathode is

$$j_{e,pass}^e = \frac{A_0 T_w^2}{2} \exp(-C' \Phi_{work}) \exp(C(\Phi_{vc} - \Phi_w)). \quad (16)$$

These two expressions enable us to relate Φ_w and Φ_{vc}

$$\begin{aligned} \Phi_w = & \Phi_{vc} - \Phi_{work} \frac{C'}{C} \\ & + \frac{1}{C} \ln \left[\frac{T_w^2 A_0}{j_{is}} \sqrt{-\frac{m_e}{8 \Phi_{vc} m_i}} \frac{1 + AG + A_r G \gamma_r / \gamma}{G} \right], \end{aligned} \quad (17)$$

where we have introduced $C' = T_e^p / T_w$. The influence of rebound on the virtual potential drop $\Phi_w - \Phi_{vc}$ is discussed further in Subsection II F, but Eq. (17) clearly shows that $\Phi_w - \Phi_{vc}$ increases with γ_r and hence with the amount of rebound electrons.

F. Virtual cathode potential drop in front of the probe

It is now instructive to examine how the virtual cathode potential drop $\Phi_w - \Phi_{vc}$ evolves with the values of the plasma parameters and the bias of the wall Φ_w . Note that an analytical expression for this potential drop cannot be straightforwardly deduced from Eq. (17), since A, A_r , and G depend on Φ_{vc} . In order to compute this potential drop, *a priori* Φ_{vc} values are set and corresponding Φ_w values are calculated from Eq. (17). Figure 2(a) displays the evolution of the potential drop $\Phi_w - \Phi_{vc}$ as a function of the bias Φ_w for different values of the plasma parameters (we recall here that potentials are normalized to the plasma electron temperature T_e^p).

A first observation is that the potential drop increases with Φ_w ; in other words, the potential well at the virtual cathode becomes shallower when the probe approaches the plasma potential. This evolution is coherent with the qualitative explanation for the formation of the virtual cathode, given in the introduction and extended in the remaining of this subsection. As Φ_w increases, all other parameters being constant, the low temperature emitted electrons are less accelerated in the sheath potential drop. If the virtual cathode potential drop were to stay constant, the flux of passing emitted electrons would stay constant (as we assume flux conservation). As their velocity at the plasma/sheath boundary would be smaller, their density at that location would increase. To maintain electroneutrality at the plasma sheath edge, a higher virtual cathode drop is necessary to filter out the slowest electrons, so that emitted electrons reaching the plasma have a higher mean velocity. This results in a lower flux and a lower density of emitted electrons at the plasma/sheath boundary. A second observation is that when the probe is significantly emissive and when its potential is close to the plasma potential, the potential drop is a non-negligible fraction of the plasma electron temperature. Thus, as the temperature of emitted electrons is usually much lower than

T_e^p , only a small fraction of the emitted electrons can override the potential barrier (the queue of the velocity distribution). It is thus clear that the emitted electron current at the wall is much larger than the passing emitted electron current, and thus than the passing plasma electron current, which justifies the assumption made at the last paragraph of Section II B—namely, to neglect true secondary emission.

Let us now investigate how the potential drop $\Phi_w - \Phi_{vc}$ evolves with the plasma parameters (see Fig. 2(a)). The plasma density is observed to be a leading parameter: the potential drop increases with decreasing plasma density. This can also be qualitatively understood from the fact that the virtual cathode shields the plasma from a flux of too slow (cold) emitted electrons. For a given emitted electron flux at the wall (T_w is fixed) and for a given wall potential, the emitted electron density at the plasma/sheath boundary is set by the virtual cathode potential drop. Decreasing the electron plasma density, all other parameters being kept constant, requires a larger virtual cathode potential drop to filter out more slow electrons and to reduce the emitted electron density at the plasma/sheath boundary to ensure quasineutrality. This evolution is observed in Fig. 2(a): the virtual cathode potential drop increases by more than 50% when the plasma density decreases from 10^{18} m^{-3} (solid black curve) to 10^{17} m^{-3} (red squares). On the other hand, the plasma electron temperature has a very weak influence on the virtual cathode potential drop $\Phi_w - \Phi_{vc}$: as potentials are normalized to T_e^p , the ratio between the 5 eV (full solid black curve) and 2.5 eV (blue bullets) data, namely, 2.11 ± 0.07 , is weakly significant. We can conclude from this that the virtual cathode potential drop strongly depends on the electron plasma density but not on the primary electron current density, in agreement with the qualitative explanation given above.

Note that for a lower value of the wall temperature (green crosses), the computation according to the space-charge limited regime predicts a negative value for the potential drop; this indeed means that the current is no more limited by the space-charge effect but simply by thermoemission.

Let us now focus on the influence of γ_r on the virtual cathode potential drop that forms in front of the emissive wall. Fig. 2(b) displays the evolution of $\Phi_w - \Phi_{vc}$ as a function of Φ_w for the reference plasma parameters and three values of γ_r . Clearly, rebound electrons have no influence when the wall potential is sufficiently negative as most of primary electrons have not enough energy to reach the wall. However, when the wall potential approaches the plasma potential, the virtual cathode potential drop increases with γ_r and, near the plasma potential, increasing γ_r from 0 to 0.8 leads to an increase by 10% of T_e^p of the virtual cathode potential drop $\Phi_w - \Phi_{vc}$ for the reference conditions. Since T_e^p is usually larger than T_e^e , it means that the fraction of emitted electrons able to override the potential barrier drops significantly, those emitted electron being replaced by primary electrons that rebound on the wall. It is of importance when considering a floating emissive probe because a non negligible part of current leaving the probe would be replaced by a current fluctuating as the plasma current (see Fig. 3 for $\gamma_r=0.3$ near the floating potential). This also has

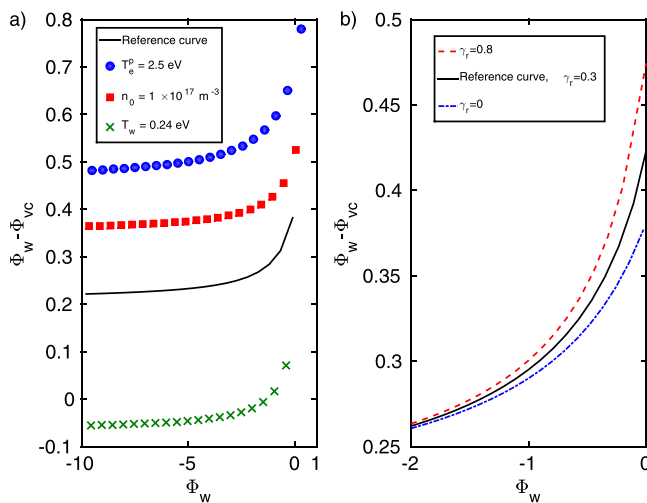


FIG. 2. Evolution of the normalized potential drop $\Phi_w - \Phi_{vc}$ as a function of the normalized bias Φ_w . The solid black lines in (a) and (b) correspond to an Argon plasma with $n_0 = 1 \times 10^{18} \text{ m}^{-3}$, $T_e^e = T_w = 0.31 \text{ eV}$, $T_e^p = 5 \text{ eV}$, $\gamma_r = 0.3$, $\phi_{\text{work}} = 4.5 \text{ eV}$, and $A_0 = 1.2 \times 10^6 \text{ A m}^{-2} \text{ K}^{-2}$ (tungsten surface). The other curves are plotted for the same parameters except for the one specified in the legend.

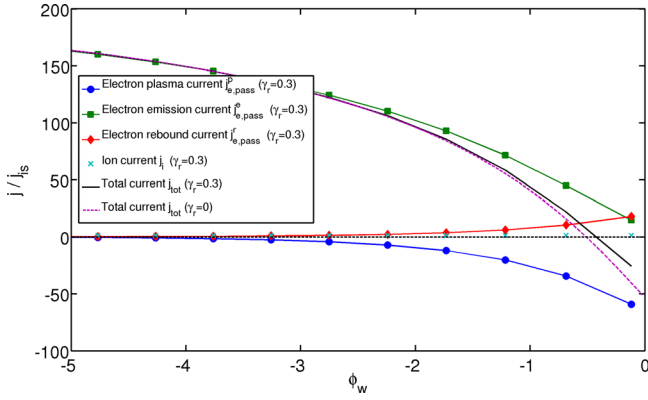


FIG. 3. Example of the different passing current densities flowing through an emissive surface under the space-charge regime. The current densities are normalized to the ion saturation current density. The calculation for the solid lines (black, green, red, light blue, and dark blue) was performed for an Argon plasma with $n_0 = 1 \times 10^{18} \text{ m}^{-3}$, $T_e^p = 5 \text{ eV}$, $T_e^e = T_w = 0.31 \text{ eV}$, $\gamma_r = 0.3$, $\phi_{\text{work}} = 4.5 \text{ eV}$, and $A_0 = 1.2 \times 10^6 \text{ A m}^{-2} \text{ K}^{-2}$ (tungsten surface). The dashed purple line corresponds to the same parameters but for $\gamma_r = 0$.

implication on thermal flux that would reach the wall as less plasma electrons are able to override the potential barrier and could be an important effect in the divertor of tokamaks, for instance.

G. I - V characteristics in the space-charge regime

From the previous computation, the total I - V characteristic of an emissive probe in the space-charge limited regime can also be computed. Once the set of parameters (Φ_{vc}, Φ_w) is known, the total current $j_{\text{tot}}(\Phi_w) = j_i + j_{e,\text{pass}}^p + j_{e,\text{pass}}^e + j_e^r$ flowing through an emissive wall biased at the associated potential Φ_w is then computed from Eqs. (2), (5), (6), and (7). An example of two I - V characteristics in the space-charge limited regime is given in Fig. 3 (solid black line for $\gamma_r = 0.3$ and dashed purple one for $\gamma_r = 0$). Note that for the case $\gamma_r = 0.3$ and in the vicinity of the floating potential ($\Phi_w \sim -0.5$), the rebound electron current reaching the probe is a significant part of the total current, on the order of the passing electron emission current. The comparison between the black solid and dashed purple lines shows that the rebound electron current increases the floating potential and modifies significantly the total current flowing through the probe near the plasma potential. It shows the importance of this electron population when dealing with emissive probes under the space-charge effect. One benefit of this computation could be to experimentally measure the coefficient of rebound electrons γ_r . Since the I - V characteristic does not depend on the true secondary emission γ_s in the space-charge limited regime, a fitting procedure of experimental characteristics would provide an estimate of γ_r , providing that the temperatures of the emissive probe (T_w) and of the emitted electrons (T_e^e) are known.

H. Virtual cathode potential for a floating hot surface under the space-charge regime

When the wall is at the floating potential, $\Phi_w = \Phi_{fl}$, there is no net current flowing through the wall, $j_{\text{tot}}(\Phi_{fl}) = 0$. For this peculiar condition, $\gamma = -j_{e,\text{pass}}^e/j_{e,\text{pass}}^p$ may be expressed

as a function of the plasma and material parameters (C , γ_r , and m_i/m_e)

$$\gamma(\Phi_{fl}) = 1 - \gamma_r - \sqrt{\frac{2\pi m_e}{m_i}} M (1 + AG + A_r G \gamma_r / \gamma) \exp(-\Phi_{vc}). \quad (18)$$

In that case, the associated virtual cathode potential is computed as the value of Φ_{vc} for which the root of the polynomial equation in G (Eq. (13)) equals the value of G given from Eq. (10) using the above expression $\gamma(\Phi_{fl})$ for its calculation. This is done numerically with a precision close to the computer precision and repeated for different sets of plasma parameters (C , γ_r , and m_i/m_e). C is varied from 1 to 100 by step of 1, γ_r from 0 to 0.8 by step of 0.01, and m_i/m_e from 1836 to 100×1836 by step of 10×1836 . We then proceed to a multivariable polynomial fit of the numerical Φ_{vc} to the seventh order of the form

$$f\left(C, \gamma_r, \frac{m_i}{m_e}\right) = \sum_{n=0}^7 \sum_{m=0}^7 \sum_{p=0}^7 a_{n,m,p} C^n \gamma_r^m \left(\frac{m_i}{m_e}\right)^p, \quad (19)$$

where $(a_{n,m,p})_{(n,m,p) \in [0,7]^3}$ are polynomial coefficients.

This leads to an estimation of Φ_{vc} that can be used to compute the floating potential Φ_{fl} in Eq. (17) for a non zero electron emission temperature T_e^e , extending the work of Hobbs and Wesson.⁹ It is worth mentioning that the discrepancy between the numerical value of Φ_{vc} and the fit is always lower than 1% for $\gamma_r \leq 0.8$ (which covers any practical situation) and that the numerical procedure ensured that the computed total current density reaching the floating wall is lower than 1% of the ion saturation current ($j_{\text{tot}} \sim 0$). Numerical computations show that increasing the density n_0 and the plasma electron temperature T_e^p or decreasing the percentage of electrons that rebound on the wall γ_r decreases the floating potential value for a given wall temperature. Consequently, the model predicts that it is more difficult to reach the plasma potential with a floating emissive material in tokamaks than in low temperature and density plasmas.

III. CONFRONTATION OF THE MODEL WITH EXPERIMENTAL RESULTS (STATIC CASE)

A. Main experimental parameters

The above theoretical model will now be compared with sets of experimental data from two experiments whose results were reported earlier. The first set of experiment was conducted in the Mirabelle device⁴ and the two others on the von-Kármán plasma machine^{5,16}—these latter sets will be referred to as VKP1 and VKP2. The mean plasma parameters of these experiments are recalled in Table I. These parameters were obtained using electrostatic probes, consisting of a small tungsten loop wire of diameter 0.2 mm with 4 mm length in the Mirabelle's case and 8 mm in the VKP experiment, operated as cold Langmuir probes. In the remaining of this article, we report measurements using these probes as emissive probes, i.e., when the tungsten loops are heated by Joule dissipation of a DC current to reach strong emission regime. The work function ϕ_{work} for the tungsten

TABLE I. Main average parameters taken from an experiment performed on the linear plasma device Mirabelle⁴ and two experiments performed on the von-Karman plasma experiment.⁵ Notice that the mean density n_0 for the Mirabelle's case is a rough estimation as a current leak in the electronic was affecting the measurement. B is the mean magnetic field at the probe position and P the neutral pressure during the discharge.

	Gas	T_e^p (eV)	ϕ_p (V)	n_0 ($\times 10^{16}$ m ⁻³)	B (mT)	P (mbar)
Mirabelle	Ar	3.6	5	[1 to 10]	30	3×10^{-4}
VKP 1	Ar	4.6	7.1	12	5	4×10^{-3}
VKP 2	Ar	5.6	12.5	9.2	5	1×10^{-3}

material is assumed to be 4.5 eV (Refs. 7 and 14) as a rough estimation, since it highly depends on surface contamination, crystal lattice, and material deformation. We take the Dushman's constant A_0 to be equal to 1.2×10^6 A m⁻² K⁻² for tungsten.⁷ Note that comparing these experimental results with a 1D space-charge model can only be viewed as a rough comparison due to the geometry of the tungsten filaments. However, the present comparison demonstrates the basic features of the space-charge limited emission model and the validity of the hypothesis used.

B. Space-charge criteria

The transition between the emission current limited by thermoemission and space-charge is controlled by the amount of emitted electrons relatively to the primary electrons. For a given set of plasma and wall parameters (material, area), the control parameter is the wall emissivity, or equivalently the wall temperature T_w when the emitted current follows the Richardson-Dushman law. The onset for the development of the virtual cathode, as already mentioned in Ref. 24, is obtained when applying the above space-charge limited model for which the virtual cathode is located at the wall $\Phi_w = \Phi_{vc}$. Assuming that the temperature of emitted electrons is that of the wall $T_e^e = T_w$ (or in other words $C = C'$), the threshold wall temperature $T_{w,t}$ is obtained using Eq. (17)

$$-\Phi_{\text{work}} + \frac{1}{C} \ln \left[\frac{A_0 T_{w,t}^2}{en_0 M c_s} \sqrt{\frac{-m_e}{8\Phi_{vc} m_i}} \frac{1 + AG + A_r G \gamma_r / \gamma}{G} \right] = 0. \quad (20)$$

This equation gives a criterion on T_w for the space-charge effect to occur depending on the plasma density n_0 and primary electron temperature T_e^p (or on j_{is} in Eq. (17)) and on the probe material emissivity (through A_0 and ϕ_{work}).

C. Experimental evidence for a transition from thermoionic to space-charge regime

In section II, experimental clues of a transition between thermoemission limited and space-charge limited regimes in the three experimental dataset mentioned above are analyzed applying the model developed in the previous section. It provides a theoretical estimate of the emissive probe temperature for this transition to occur. In Fig. 3 of Ref. 4 and from Figs. 5 and 3 of Ref. 5, the experimentally measured standard deviation of the floating potential of an emissive probe

follows quite well the theoretical standard deviation as calculated from the model for the temperature limited emission regime, up to a given emission current (or equivalently a given wall temperature). Then, the experimental points depart significantly from this model, meaning that the model assuming thermoemission limited current is no more valid. This transition is supposed to be related to a transition to space-charge limited emission. In particular, this is observed in Fig. 3 of Ref. 4, as the emission current I_{em} is greater than 1 mA and in Figs. 5 and 3 of Ref. 5, as $I_{em} \sim 20$ mA for the dataset VKP2 or less clearly as $I_{em} \sim 30$ mA for the dataset VKP1.

The key experimental parameters at the transition (i.e., the emission current I_{em}^t and the corresponding probe potential $\phi_{w,t}$) are reported in the first two columns of Table II. By inputting in Eq. (20) the experimental values given in Table I, the emitted electron temperature at the transition $T_{w,t}$ is estimated. We also assume here that $T_w = T_e^e$ (leading to $C' = C$). The theoretical value of the wall potential at the transition is obtained as $\phi_{w,t} = \phi_{vc}(T_{w,t})$ using the multi-variable polynomial fit for calculating $\phi_{vc}(T_{w,t})$. These theoretical values are reported in the rightmost columns of Table II. The probe temperatures at the transition computed from the model lie between 2300 and 2500 K for the three experiments, which are reasonable values. The theoretical values of $\phi_{w,t}$ lie in the transition interval observed experimentally. This is in agreement with the interpretation of the regime change observed experimentally and the transition towards space-charge limited regime and with Eq. (17) holding for values of I_{em} above I_{em}^t .

D. Average emissive probe potential in the space-charge limited regime

For heating currents above I_{em}^t (i.e., in the space-charge current limited regime), the floating potential of the probe of the aforementioned experiments is predicted using the polynomial fit of Φ_{vc} (Eq. (19)) in Eq. (17). However, this prediction requires the knowledge of T_w and T_e^e . Since none of these parameters were experimentally accessible, the following procedure is adopted: we first assume $T_w = T_e^e$ and then the evolution of the floating probe potential is computed for two values of T_w , namely, at the onset of the space-charge regime ($T_w \sim 2550$ K = 0.22 eV), and tungsten melting point ($T_w \sim 3700$ K = 0.32 eV). The evolution of the predicted probe floating potential value as a function of γ_r is shown in Fig. 4 for the two aforementioned temperature T_w . Together with these predicted theoretical values, Fig. 4 displays the plasma potential value ϕ_p measured from analysis of cold

TABLE II. Transition parameters I_{em}^t and $\Phi_{w,t}$ estimated from the data of Refs. 4 and 5 and theoretical values estimated using the criteria of Eq. (20) assuming $T_w = T_e^e$. The density in the Mirabelle's case is taken to be 5×10^{16} m⁻³. We assume the parameter γ_r to be equal to 0.3.

	Exp. I_{em}^t (mA)	Exp. $\phi_{w,t}$ (V)	Th. $T_{w,t}$ (K)	Th. $\phi_{w,t}$ (V)
Data Mirabelle	0.9–1.1	1.2–1.9	2340	2.2
Data 1 VKP	30–35	3.5–4.1	2450	3.5
Data 2 VKP	15–20	7.1–8.6	2420	8.1

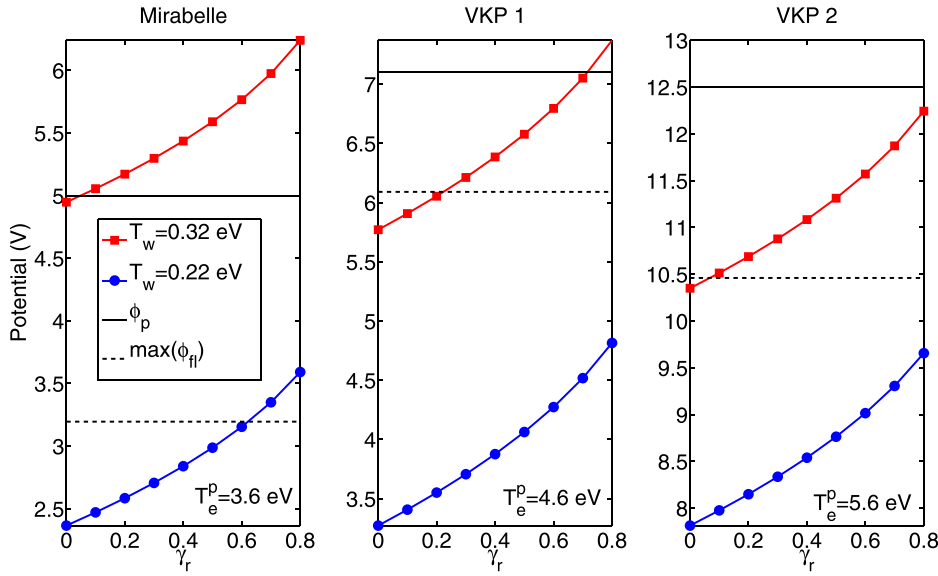


FIG. 4. Average floating potential obtained with Eq. (17) assuming $T_w = T_e^c$ and using data from Table I. Left: Mirabelle experiment, center: VKP 1, right: VKP 2. The floating potential $\phi_{fl,max}$ corresponds to the maximum of the probe floating potential obtained experimentally. The plasma potential ϕ_p was obtained from cold probe analysis.

Langmuir probes I - V characteristics as well as the average values of the probe floating potential $\phi_{fl,max}$ measured from emissive probes that correspond to the maximum values of the emission current I_{em} achieved in the three experiments.

For the three cases under investigation, the experimental probe floating potentials lie within the range of floating potential predicted from theory (which indeed strongly depends on T_w and γ_r). In the Mirabelle's case, the maximum floating potential achieved experimentally lies in between the two circled blue and squared red curves even for a zero $\gamma_r = 0$ (no rebound electrons). However, even for the highest probe temperature ($T_w = 0.32$ eV at the melting point), the model cannot explain the VKP experimental observations if no rebound electrons are considered. This clearly shows the importance of taking into account rebound electrons in the derivation of the model.

IV. INFLUENCE OF PLASMA PARAMETER FLUCTUATIONS ON FLOATING EMISSIVE PROBE FLUCTUATIONS IN THE SPACE-CHARGE LIMITED REGIME

The floating potential of an emissive probe emitting enough electrons to float near the plasma potential mean value is usually believed to measure fluctuations of the plasma potential. However, it has recently been demonstrated in Refs. 4 and 5 that plasma density and electron temperature fluctuations also play a role in the floating potential of the probe. In the two aforementioned articles, it has been explained theoretically why it is so when the emission current is limited by thermoemission but not when the probe is under the space-charge regime. In this section, the sheath model in the space-charge current limited regime derived in Section II is applied to the experimental data to see the influence of both electron density and temperature fluctuations on using the probe potential. The influence of the rebound electrons on the dynamics of the fluctuations of the floating potential is also discussed.

A. First order expansion from the model

The model presented in Section II was derived for static plasma parameters. However, as emissive probe measurements are usually used to probe low frequency fluctuations of the plasma potential, we use the model to account for the effect of slow plasma parameter fluctuations (i.e., fluctuations whose frequency is much smaller than the ion plasma frequency). To get an insight into the influence of the fluctuations of T_e^p and n_0 on the probe, a first order expansion of Eq. (17) is done. In the following, the wall temperature T_w is assumed to be constant as thermal frequency responses of the material are much slower than plasma fluctuation frequencies of interest (in the kiloHertz range) and $T_e^c = T_w$ is once again assumed. A first order expansion of the floating potential reads

$$\begin{aligned} \Delta\phi_{fl} &= \frac{\partial\phi_{fl}}{\partial\phi_p} \Delta\phi_p + \frac{\partial\phi_{fl}}{\partial\bar{n}} \Delta\bar{n} + \frac{\partial\phi_{fl}}{\partial T_e^p} \Delta T_e^p \\ \Rightarrow \Delta\bar{\phi}_{fl} &= \frac{\Delta\phi_{fl}}{\langle T_e^p \rangle} = \frac{\partial\phi_{fl}}{\partial\phi_p} \Delta\bar{\phi}_p + \frac{\partial\bar{\phi}_{fl}}{\partial\bar{n}} \Delta\bar{n} + \frac{\partial\phi_{fl}}{\partial T_e^p} \Delta\bar{T}_e^p, \end{aligned}$$

where \bar{f} means normalized quantities (the density is normalized to $\langle n_0 \rangle$, while potentials and electron temperature are normalized to $\langle T_e^p \rangle$), and $\langle \rangle$ stands for the mean value. The relative amplitudes of $\partial\bar{\phi}_{fl}/\partial\bar{n}$ and $\partial\phi_{fl}/\partial T_e^p$ are compared to $\partial\phi_{fl}/\partial\phi_p = 1$ in Subsection IV A 1 and IV A 2.

1. Plasma density fluctuations

The dependence of $\bar{\phi}_{fl}$ on the plasma density is readily estimated as $\bar{\phi}_{vc}$ depends only on $C = T_e^p/T_w$ (m_i/m_e is a constant and γ_r is supposed to remain constant during one given experiment). The plasma density then only appears in j_{is} (Eq. (17)). Doing a first order Taylor expansion by setting $n_0 = \langle n_0 \rangle + \delta n_0$ with $\delta n_0 \ll \langle n_0 \rangle$, one get $\partial\bar{\phi}_{fl}/\partial\bar{n} = -1/\langle C \rangle$. In low temperature plasmas $\langle C \rangle = \langle T_e^p \rangle/T_w \in [6 - 20]$ which leads to a discrepancy of about 5%–15% in the measurement of the plasma potential fluctuations. Note that in tokamak $\langle C \rangle \gg 100$ so that according to our 1D

model, density fluctuations do not affect emissive probe measurements in the space-charge limited regime.

2. Plasma temperature fluctuations

The influence of plasma temperature fluctuations on the floating potential of the probe can only be computed numerically as the dependence of Φ_{vc} upon C is non-trivial. Looking at Eq. (17), one can notice that five parameters affect Φ_{fl} : T_e^p , T_w , γ_r , m_i/m_e , n_0 as A_0 is set to 1.2×10^6 A m⁻² K⁻² for the tungsten wall. $\partial\phi_{fl}/\partial T_e^p$ is then computed for different sets of parameters, changing one parameter at a time and for a wide range of mean plasma temperature value T_e^p . The results are as follows.

First, $\partial\phi_{fl}/\partial T_e^p$ hardly depends on the wall temperature T_w (or equivalently C since we assume $T_w = T_e^e$) nor on the plasma density $\langle n_0 \rangle$. This has been tested by changing T_w from 0.22 eV (onset value for space-charge regime to occur) to its highest value for tungsten (0.32 eV) and by increasing $\langle n_0 \rangle$ by three orders of magnitude (from 10^{17} m⁻³ up to 10^{20} m⁻³ to reach tokamak values). In all cases, $\partial\phi_{fl}/\partial T_e^p$ remains quite unchanged, so we conclude that both parameters T_w and n_0 have a very weak influence on floating potential fluctuations.

The effect of the gas mass is rather weak. From an Argon (like Mirabelle and VKP discharges presented here) to a Hydrogen plasma (in tokamak for instance), the influence of temperature fluctuations on ϕ_{fl} would only be diminished by less than 5%. However, changing the rebound coefficient γ_r has a much stronger effect as one can see in Fig. 5. Increasing the value of γ_r from 0 to 0.7 decreases the influence of temperature fluctuations by about 25% when T_e^p is high enough. For a reasonable value of γ_r , i.e., 0.3, the fluctuations would be diminished by more than 10% compared to $\gamma_r = 0$. The fact that the influence of temperature fluctuations diminishes with γ_r can be easily understood as

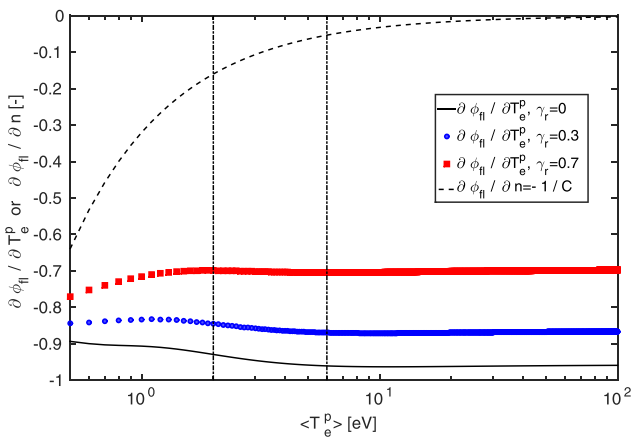


FIG. 5. Variation of the partial derivative of ϕ_{fl} with respect to the plasma temperature T_e^p as a function of $\langle T_e^p \rangle$. Each curve was calculated by numerically differentiating Eq. (17). The black solid line is obtained for an Argon gas, $\langle n_0 \rangle = 1 \times 10^{17}$ m⁻³, $\gamma_r = 0$, $T_w = T_e^e = 0.25$ eV, and $A_0 = 1.2 \times 10^6$ A m⁻² K⁻². The circled blue and the squared red curves are plotted for the same parameters except for γ_r that is changed to 0.3 and 0.7, respectively. For comparison, we also display the partial derivative of $\bar{\phi}_{fl}$ with respect to the normalized density \bar{n} (the black dashed line, $-1/C$) for $\langle T_e^e \rangle = 0.32$ eV as well as the $\langle T_e^e \rangle$ boundaries corresponding to low temperature plasmas (2–6 eV—vertical dashed lines).

increasing γ_r results in replacing slow emission electrons by fast rebound electrons whose current compensates exactly a fraction of the current of primary electrons that fluctuates with $\langle T_e^p \rangle$.

Then, one can notice that $\partial\phi_{fl}/\partial T_e^p$ for all the curves in Fig. 5 quickly saturates to some constant value by increasing $\langle T_e^p \rangle$, meaning that the fluctuations of temperature affect ϕ_{fl} in low, as well as in high, temperature plasmas. Last but not least, temperature fluctuations have a much stronger influence on $\bar{\phi}_{fl}$ than density ones as $\partial\phi_{fl}/\partial T_e^p$ is much greater (in absolute value) than $\partial\bar{\phi}_{fl}/\partial \bar{n} = -1/\langle C \rangle$ shown by a dashed line in Fig. 5. The contribution of temperature fluctuations on the floating potential is actually quite significant with respect to the ones of the plasma potential fluctuations (a bit lower in absolute value). This means that ϕ_{fl} fluctuations are strongly affected by T_e^p fluctuations and thus that the floating potential fluctuations of an emissive probe differs from the ones of the plasma potential according to the model, even though reduced by taking into account γ_r .

B. Comparison to experimental data: VKP data

In this subsection, the experimental floating potential fluctuations measured by an emissive probe under the space-charge limited current regime are compared to the fluctuations given by the model derived in Section II (Eq. (17)), the experimental fluctuations of the plasma parameters (T_e^p , n_e , and ϕ_p) being the inputs of the model. Data obtained on Mirabelle could not be processed since the time evolution of the temperature was not measured and density fluctuations measurements were not precise enough. We thus focus on the VKP experiment⁵ for which, a conditional reconstruction method of the I - V characteristics¹⁷ has been used, enabling the measurements of all the interesting time series (T_e^p , n_e , ϕ_{fl} , ϕ_p , and $\phi_{fl,em}$). The only drawback of this experiment could lie in the way the plasma is created in the VKP device: using radiofrequency coupling. Thus, the electron temperature could be over estimated and there could be errors on its phase measurements—although previous measurements with compensated cold Langmuir probes^{6,22} did not show significant differences with measurements with uncompensated cold Langmuir probes. The time series used here are those shown in Fig. 4 of Ref. 5, corresponding to emission regimes when the mean floating potential was the closest to the plasma potential (i.e., for the largest emission current). In both cases, according to results shown in Section III C of this article, the current is obviously space-charge limited. The experimental fluctuations of the floating potential obtained in both regimes are shown as blue square symbols in both panels of Fig. 6. The associated plasma potential fluctuations are displayed as black circles. In order to compare these time-series to the space-charge model, $T_w = T_e^e$ is assumed and γ_r is set to a realistic value of 0.3. T_w is computed to ensure equality between the mean potential found using the space-charge model and the experimental data, leading to $T_w = 0.31$ eV for both experiments. The theoretical curves correspond to the red curves in Fig. 6.

In the first experiment, the standard deviation given by the model is 0.062 V while experimentally it is about

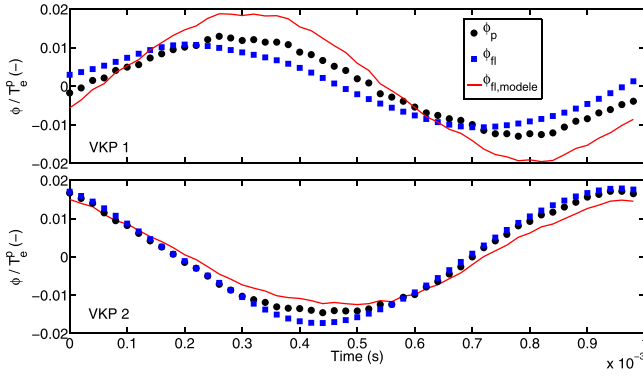


FIG. 6. Fluctuations of the normalized plasma potential (black dots), experimental floating potential (blue squares), and theoretical floating potential (red solid lines) as a function of time for (a) VKP1 and (b) VKP2. The theoretical red curves are calculated using the experimental time series plugged in Eq. (17) and assuming $T_w = T_e^e$. In (a) and (b), we used $T_w = 0.31$ eV and $\gamma_r = 0.3$.

0.035 V, and in the second, the modeled standard deviation is 0.054 V for an experimental one of 0.069 V (see Table III). This discrepancy between the model and the experimental data cannot be explained by the choice of the *a priori* value we took for T_w and γ_r . We have shown in Sec. IV A that changing T_w does not affect much the standard deviation, in agreement with the experimental data under the space-charge regime for which changing I_{em} , so T_w , does not affect much the standard deviation (see Figs. 3 and 5 of Ref. 5). However, we shown in the same section that changing γ_r affects the floating potential fluctuations. In Table III, it can be seen that changing γ_r from 0 to 0.7 affects the modeled standard deviation of about 11% in VKP 1 and 5% in VKP 2. Even though significant, the rebound electrons do not suffice to explain the discrepancy between the model and the experimental data. More experimental verification (where the 1D assumption would be more accurate to match the model) or theoretical developments including more complex geometries should be investigated to draw any clear conclusion. Nevertheless, rebound electrons would certainly be an important ingredient as they replace part of the emitted current by a current fluctuating like the electron plasma current.

V. CONCLUSIONS AND DISCUSSIONS

In this article, an improved version of the 1D model developed by Takamura²³ is presented. Namely, the modeling of the total current flowing through an emissive probe under the space-charge regime is modified by taking into account

TABLE III. Experimental and theoretical standard deviations of the floating potential of the emissive probe for the two VKP experiments. The theoretical ones are calculated using the experimental time series plugged in Eq. (17) and setting $T_w = T_e^e$ to 0.31 eV.

	VKP 1 (V)	VKP 2 (V)
Experiment	0.035	0.069
Model $\gamma_r = 0$	0.065	0.053
Model $\gamma_r = 0.3$	0.062	0.054
Model $\gamma_r = 0.7$	0.058V	0.056

secondary electron emission due to the retrodiffusion of primary electrons on the hot surface. We then proceed to obtain a relation linking the probe potential to the virtual cathode potential. From this relation, we derive a criterion on the wall temperature with respect to the plasma and wall parameters for the transition between thermoemission to space-charge regimes to occur. Last, in the peculiar case of the floating potential, a numerical estimation of the virtual cathode potential is obtained for a large range of experimental parameters. This allows us to apply the model to experimental floating potential data from two different experiments.

We first show in Section III the importance of taking into account rebound electrons in the model derivation to reproduce the mean floating potential of the experimental observations. We also show that the transition between the thermoemission regime to the space-charge one agrees with the previous observations^{4,5} and appears for probe temperatures around 2300–2500 K. More systematic experiments could be done to verify this last point by measuring experimentally the probe temperature. In addition, tests with different probe materials, thus changing the work function and the wall temperature transition value, could also provide useful information.

Then, we study the effect of low frequency plasma parameter fluctuations (compared to the plasma ion frequency) on the floating potential of an emissive probe given by the static space-charge model. The model shows that plasma density fluctuations have a very weak effect for low temperature plasmas (2–5 eV) and are completely negligible for high temperature plasmas (>5 eV, tokamaks). Thus, plasma density fluctuations hardly contribute to floating potential fluctuations. Plasma temperature fluctuations, however, have a non-negligible effect on the probe floating potential meaning that inferring plasma potential fluctuations from emissive probes would not be straightforward. Nevertheless, according to this model, taking into account rebound electrons results in a lower influence of plasma electron temperature fluctuations, whose influence decreases with γ_r .

We then proceed to compare the 1D model with the experimental low floating potential fluctuations of an emissive probe under the space-charge regime. Unfortunately, the theory does not properly model fluctuations of the floating potential. To gain further insight into the model validity, the experimental results using controlled driving of harmonic fluctuations presented here should be extended in the future to situations where the time evolution of the electron temperature is probed with a high accuracy. Moreover, the 1D theoretical model was applied to experiments where 2D effects are unavoidable (potential gradient along the tungsten filament).¹⁵ In a foreseen work, the plane surface LaB6 probe heated by the laser, as suggested by Schrittwieser *et al.*,¹⁹ should be used. In that case, the mean potential on the probe surface is homogeneous, as no strong DC current circulates in the probe.

ACKNOWLEDGMENTS

This work has been partly funded by the French National Research Agency under the two Contract Nos. ANR-13-JS04-0003-01 and ANR-11-BS09-023-03 Sediba.

- ¹Fusion research in Austria - activities report in 2014 and 2015; available at http://www.oeww.ac.at/fileadmin/subsites/etc/FusionOEAW/PDF/Fusion_Research_in_Austria_14-15.pdf.
- ²J. Adamek, J. Horacek, J. Seidl, H. W. Muller, R. Schrittwieser, F. Mehlmann, P. Vondracek, S. Ptak, COMPASS Team, and ASDEX Upgrade Team, "Direct plasma potential measurements by ball-pen probe and self-emitting Langmuir probe on compass and ASDEX Upgrade," *Contrib. Plasma Phys.* **54**(3), 279–284 (2014).
- ³G. Bousselin, J. Cavalier, J. F. Pautex, S. Heuraux, N. Lemoine, and G. Bonhomme, "Design and validation of the ball-pen probe for measurements in a low-temperature magnetized plasma," *Rev. Sci. Instrum.* **84**, 013505 (2013).
- ⁴G. Bousselin, N. Lemoine, J. Cavalier, S. Heuraux, and G. Bonhomme, "On the measurement of plasma potential fluctuations using emissive probes," *Rev. Sci. Instrum.* **85**, 056102 (2014).
- ⁵G. Bousselin, N. Plihon, N. Lemoine, J. Cavalier, and S. Heuraux, "How plasma parameters fluctuations influence emissive probe measurements," *Phys. Plasmas* **22**, 053511 (2015).
- ⁶A. Cantin and R. Gagne, *Appl. Phys. Lett.* **30**, 316 (1977).
- ⁷V. S. Fomenko, *Handbook of Thermoionic Properties: Electronic Work Functions and Richardson Constants of Elements and Compounds* (Plenum Press Data Division, 1966).
- ⁸J. P. Gunn, "Evidence for strong secondary electron emission in the tokamak scrape-off layer," *Plasma Phys. Controlled Fusion* **54**, 085007 (2012).
- ⁹G. D. Hobbs and J. A. Wesson, "Heat flow through a Langmuir sheath in the presence of electron emission," *Plasma Phys.* **9**, 85–87 (1967).
- ¹⁰R. F. Kemp and J. M. Sellen, *Rev. Sci. Instrum.* **37**, 455 (1966).
- ¹¹I. H. Khan, J. P. Hobson, and R. A. Armstrong, "Reflection and diffraction of slow electrons from single crystals of tungsten," *Phys. Rev.* **129**(4), 1513–1523 (1963).
- ¹²I. Langmuir, *Phys. Rev.* **21**, 419 (1923).
- ¹³W. Li, J. X. Ma, J. Li, Y. Zheng, and M. Tan, *Phys. Plasmas* **19**, 030704 (2012).
- ¹⁴H. B. Michaelson, "The work function of the elements and its periodicity," *J. Appl. Phys.* **48**(11), 4729–4733 (1977).
- ¹⁵E. Mravlag and P. Krumm, "Space potential measurements with a continuously emitting probe," *Rev. Sci. Instrum.* **61**, 2164 (1990).
- ¹⁶N. Plihon, G. Bousselin, F. Palermo, J. Morales, W. J. T. Bos, F. Godeferd, M. Bourgoïn, J.-F. Pinton, M. Moulin, and A. Aanesland, "Flow dynamics and magnetic induction in the von-Karman plasma experiment," *J. Plasma Phys.* **81**, 345810102 (2015).
- ¹⁷N. Plihon, C. S. Corr, P. Chabert, and J. L. Raimbault, "Periodic formation and propagation of double layers in the expanding chamber of an inductive discharge operating in Ar/SF 6 mixtures," *J. Appl. Phys.* **98**(2), 1–7 (2005).
- ¹⁸B. S. Schneider, S. Costea, C. Ionita, R. Schrittwieser, V. Naulin, J. J. Rasmussen, R. Starz, N. Vianello, J. Kovacic, and T. Gyergyek, "Robust highly emissive probe for plasma potential measurements in the edge region of toroidal plasmas," *Proc. Sci.* (2015); available at <http://pos.sissa.it/cgi-bin/reader/contribution.cgi?id=240/072>.
- ¹⁹R. Schrittwieser, C. Ionita, P. Balan, R. Gstrein, O. Grulke, T. Windisch, C. Brandt, T. Klinger, R. Madani, G. Amarandei, and A. K. Sarma, "Laser-heated emissive plasma probe," *Rev. Sci. Instrum.* **79**, 083508 (2008).
- ²⁰J. P. Sheehan and N. Hershkowitz, "Emissive probes," *Plasma Sources Sci. Technol.* **20**(6), 063001 (2011).
- ²¹A. Siebenforcher and R. Schrittwieser, "A new simple emissive probe," *Rev. Sci. Instrum.* **67**, 849 (1996).
- ²²I. D. Sudit and F. F. Chen, "Rf compensated probes for high-density discharges," *Plasma Sources Sci. Technol.* **3**(2), 162 (1994).
- ²³S. Takamura, N. Ohno, M. Y. Ye, and T. Kuwabara, "Space-charge limited current from plasma-facing material surface," *Contrib. Plasma Phys.* **44**(1–3), 126–137 (2004).
- ²⁴M. Y. Ye and S. Takamura, "Effect of space-charge limited emission on measurements of plasma potential using emissive probes," *Phys. Plasmas* **7**, 3457–3463 (2000).